

Saddle-Node Bifurcation and Homoclinic Persistence in AFM with Periodic Forcing

Alexander Gutierrez G.*, Daniel Cortés Z.†, Diego A. Castro G.‡

Abstract We study the dynamics of an Atomic Force Microscope (AFM) model, under the Lennard-Jones force with non-linear damping, and harmonic forcing. We establish the bifurcation diagrams for equilibria in a conservative system. Particularly, we present conditions that guarantee the local existence of saddle-node bifurcations. By using the Melnikov method, the region in the space parameters where the persistence of homoclinic orbits is determined in a non-conservative system.

Keywords: Homoclinic Orbits, Bifurcation, Melnikov's function.

1 Introduction

The Atomic Force Microscopes (AFMs), were created in 1986 by Binnig, et. al, [19]. They are based on the tunneling microscope and the needle profilometer principles. Generally, AFMs measure the interactions between particles by allowing the nanoscale study of the surfaces for different materials, [7, 9, 16]. In fact a wide variety of applications in analysis of pharmaceutical products, the study of the properties of fluids and fluids in cellular detection, the medicine studies, among others can be found in [5, 6, 18, 20].

The model is presented in [2, 3], where the authors study the interaction between the sample and the device's tip, see figure 1. The associated differential equation is:

$$\ddot{y} + \frac{C}{(y+a)^3} \dot{y} + y = \frac{b_1}{(y+a)^8} - \frac{b_2}{(y+a)^2} + f(t). \quad (1)$$

where b_1, b_2 and a are positive constants and f is a continuous function T -periodic with zero average, that is, $\bar{f} = \frac{1}{T} \int_0^T f(t) dt = 0$. The right hand side

$$F_{LJ} := \frac{b_1}{(y+a)^8} - \frac{b_2}{(y+a)^2},$$

is known as the Lennard-Jones force, which can be considered as a simple mathematical model to explain the interaction between a pair of neutral atoms

*Universidad Tecnológica de Pereira (UTP), alexguti@utp.edu.co

†Universidad Tecnológica de Pereira (UTP), danielcortezapata@utp.edu.co

‡Universidad Tecnológica de Pereira (UTP), xandercastro@utp.edu.co

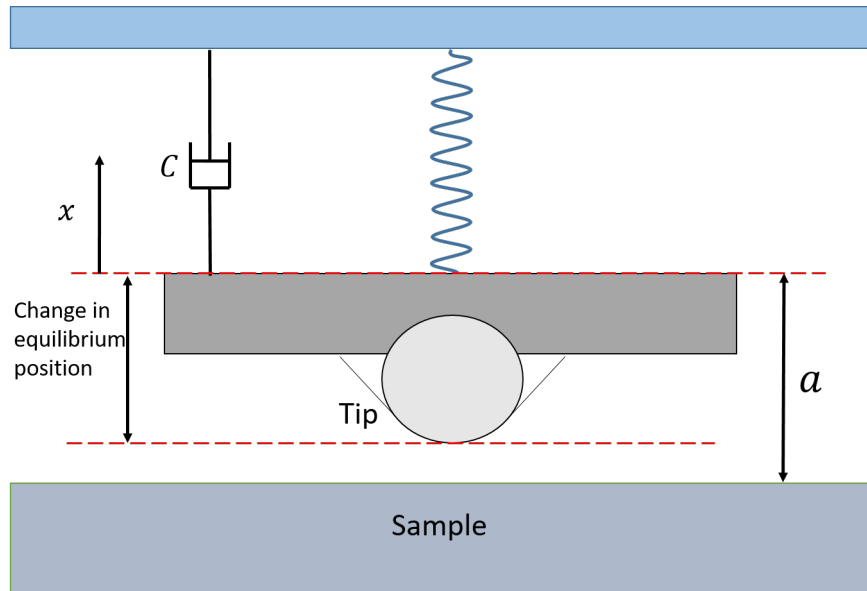


Figure 1: Mechanical model associated with the AFM's devices.

or molecules; see [13, 15] for the standard formulation. The first term describes the short-range repulsive force due to overlapping electron orbits so-called Pauli repulsion, whereas the second term simulates the long-range attraction due to van der Waals forces. This is a special case of the wider family of Mie forces

$$F_{n,m}(x) = \frac{A}{x^n} - \frac{B}{x^m},$$

where n, m are positive integers with $n > m$, also known as the $n - m$ Lennard-Jones force, see [8]. On the other hand, the dissipative term of (1):

$$F_r = \frac{C}{(y + a)^3} \dot{y},$$

is associated with a damping force of compression squeeze-film type. In specialized literature, compression film type damping can be considered as the most common and dominant dissipation in different mechanisms, (see [22, 23] and their bibliography).

For the conservative system, two main results were obtained, Theorems 1 and 2, where we establish analytically the bifurcation diagram of the equilibria for specific regions with the involved parameters in contrast to the one obtained in [12]. In particular, Theorem 2 proves the local existence of two saddle-node bifurcations that can be related to hysteresis phenomenon, see for example [4, 24].

In the non-conservative system, we present as a main result, Theorem 4, which gives a thorough and rigorous condition for the persistence of homoclinic orbit when the external forcing is of the form $f(t) = B \cos(\Omega t)$. The condition found relates the amplitude of the external forcing B with the damping constant C , which in practice can be used to prevent the AFM device from becoming decalibrate.

This article is structured in the following way: this first section as an introduction, section two is dedicated to prove the main results in conservative system, and section three contains the proof for the main result of the non-conservative system along with some illustrative examples.

2 Bifurcation Diagrams

With the change of variable $x = y + a$, (1) is rewritten as

$$\ddot{x} = m(x) + a + \epsilon \left(f(t) - \frac{C}{x^3} \dot{x} \right), \quad (2)$$

where $m(x) = \frac{b_1}{x^8} - x - \frac{b_2}{x^2}$ is the total force acting over the system, which is a combination of the Lennard-Jones force and the restoring force of the oscillator. The change of the singularity from $-a$ to 0 will facilitate the study of the bifurcation diagram for equilibria in the conservative system ($\epsilon = 0$). Note that the classification of the equilibrium solutions of (2) plays an important role when the full equation is studied. We now describe some properties of the function $m(x)$:

$$\lim_{x \rightarrow 0^+} m(x) = \infty, \quad \lim_{x \rightarrow \infty} \frac{m(x)}{x} = -1,$$

moreover m has only one positive root and a direct analysis provides a critical value

$$b_1^* = \frac{4}{27} b_2^3, \quad (3)$$

such that:

- i) If $b_1 > b_1^*$, then $m(x)$ is decreasing.
- ii) If $b_1 = b_1^*$, then $m(x)$ is non-increasing and has an inflection point in $x_c = (\frac{4}{3} b_2)^{1/3}$.
- iii) Finally, if $b_1 < b_1^*$, then $m(x)$ has a local maximum (resp. minimum) in x_r (resp. x_l) and $m(x_r), m(x_l) < 0$.

Therefore, the equilibria set $\mathcal{G} = \{x \in \mathbb{R}^+ : m(x) + a = 0\}$ is finite, not empty, and the number of equilibria depends on the parameter a . Figure 2, shows the possible variants of the m function in terms of b_1 , b_2 and a .

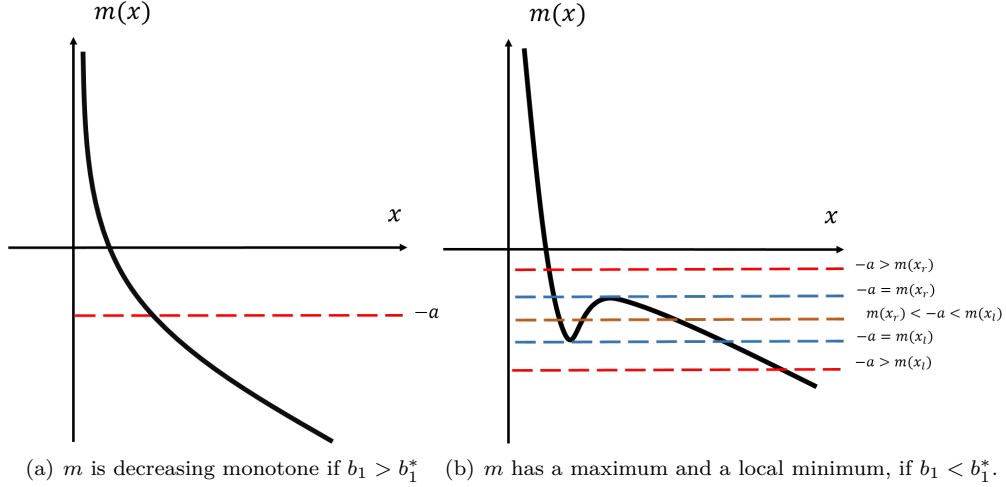


Figure 2: The m function in terms of parameters b_1, b_2 .

The proof of Theorem 1 will be made by establishing the equilibria for system (2). Let us define the energy function:

$$E(x, v) := \frac{v^2}{2} + \frac{x^2}{2} + \frac{1}{7} \frac{b_1}{x^7} - \frac{b_2}{x} - ax. \quad (4)$$

Note that the local minimums of E correspond to non-linear centers and the local maximums correspond to saddles. However, when E has a degenerate critical point $(x^*, 0)$, since the Hessian matrix A is such that $\text{Tr}A = 0$, $\text{Det} A = 0$, but $A \neq 0$. In this case, [1] shows, that the system can be written in "normal" form:

$$\begin{aligned} \dot{x} &= y \\ \dot{y} &= a_k x^k [1 + h(x)] + b_n x^n y [1 + g(x)] + y^2 R(x, y), \end{aligned} \quad (5)$$

where $h(x)$, $g(x)$ and $R(x, y)$ are analytic in a neighborhood of the equilibrium point $h(x^*) = g(x^*) = 0$, $k \geq 2$, $a_k \neq 0$ and $n \geq 1$. Thus the degenerate critical point $(x^*, 0)$ is either a focus, a center a node, a (topological) saddle, saddle-node, a cup or a critical point with an elliptic domain, see [17, Theorem 2, pp 151, Theorem 3, pp 151].

Theorem 1. *The equilibrium solutions of the conservative system associated with (2) are classified as follows:*

1. A non-linear center if either $b_1 \geq b_1^*$ and $a \in \mathbb{R}^+$ or $b_1 < b_1^*$ and $a \in \{\mathbb{R}^+ - \} - m(x_r), -m(x_l)[$.
2. Two non-linear centers and a saddle if $b_1 < b_1^*$ and $a \in] -m(x_r), -m(x_l)[$.
3. A non-linear center and a cusp, if either $b_1 < b_1^*$ and $a = -m(x_r)$ or $a = -m(x_l)$.

Proof. We present here the main steps 1. – 3. of the argument.

1. Note that \mathcal{G} has a unique element if either $b_1 > b_1^*$ and $a \in \mathbb{R}^+$ or $b_1 < b_1^*$ and $a \in \mathbb{R}^+ -] - m(x_r), -m(x_l)[$, the equilibrium is a non-linear center since E reaches a local minimum at that point. For the case $b_1 = b_1^*$, $a = -m(x_c)$ is degenerate, using the expansion given in (5), we have $k = 3$ and

$$a_k = \frac{24 b_2}{6 x_c^5} - \frac{720 b_1^*}{6 x_c^{11}} < 0,$$

therefore, from [17, Theorem 2, pp 151], follows that the equilibrium is a non-linear center.

2. Under the hypothesis made, the set \mathcal{G} has three solutions such that two are local minimums of E and the other is a local maximum of E . Consequently, two of the equilibria are non-linear centers and the other equilibrium is a saddle.

3. In this case, \mathcal{G} has two solutions such that one of them is a local minimum of E and corresponds to a non-linear center while the other one is degenerate with $k = 2$, $b_1 = 0$ in (5). Consequently, [17, Theorem 3, pp 151] guarantees that equilibrium is a cusp. \square

In the next section, we focus on the persistence of homoclinic orbits present in Theorem 1 when studying the equation (2).

The conservative equation associated with (2) can be written as the parametric system:

$$\begin{aligned} x' &= y \\ y' &= F(x, a), \end{aligned} \tag{6}$$

where $F(x, a) = m(x) + a$. Note that Theorem 1 allows us to build the bifurcation diagram of equilibria in terms of the parameter a , see figures 2 and 3. Moreover, when $b_1 \geq b_1^*$ the parameter a does not modify the dynamics of the system as it does when $b_1 < b_1^*$. In fact, there exists numerical evidence, see [3, 22], which shows that the points (x_i, a_i) , with $a_i = -m(x_i)$, $i = r, s$ are bifurcation points. In the following theorem, it will be formally shown that those points are saddle-node bifurcation points.

Theorem 2. *If $b_1 < b_1^*$ then the points (x_i, a_i) , $i = r, l$ are local saddle-node bifurcation for the conservative system (2).*

Proof. In fact, it is enough that the following conditions are fulfilled, as shown in [14, Theorem 3.1, pp 84]:

$$\text{A1 } \partial_{xx} F(x, a)|_{(x_i, a_i)} \neq 0.$$

$$\text{A2 } \partial_a F(x, a)|_{(x_i, a_i)} \neq 0.$$

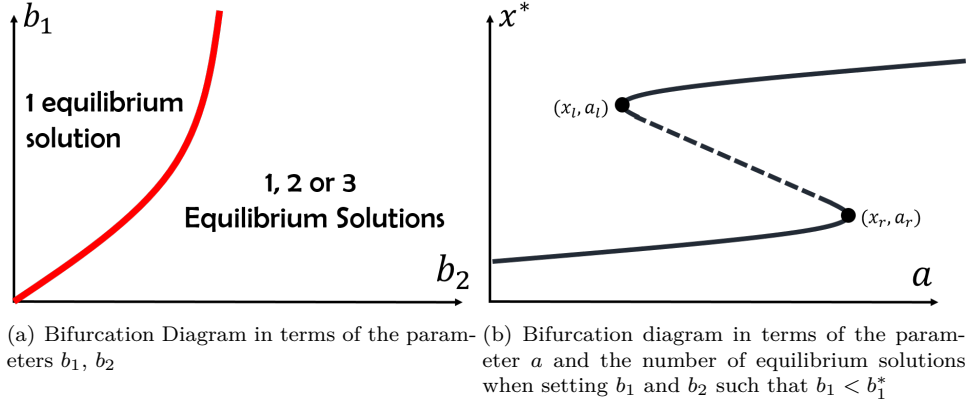


Figure 3: Bifurcation Diagrams of the equation (2) in conservative system.

Indeed, we have $\partial_{xx}F(x, a)|_{(x_l, a_l)} > 0$ (resp. $\partial_{xx}F(x, a)|_{(x_r, a_r)} < 0$), because m has relative minimum (resp. maximum) in x_l (resp. x_r) and $\partial_a F(x, a)|_{(x_i, a_i)} = 1$. \square

To summarize, the results obtained in theorems 1 and 2 are illustrated in the bifurcation diagram of the conservative system associated to (2). In part a) of Figure 3 the red curve separates the region in terms of the parameters b_1 and b_2 for which the conservative system has a unique equilibrium (independent of the parameter a), of the region where the number of equilibrium solutions depends on the parameter a . In fact, if we take $(b_2, b_1) \in \mathbb{R}_+^2 - \{(b_2, b_1) \in \mathbb{R}_+^2 : b_1 \geq b_1^*\}$ then the conservative system may have one, two or three equilibria as illustrated in Figure 3 (b). In this figure the solid lines are related to the stable equilibria, while the dotted line is related to the solutions of unstable equilibria. Furthermore it can be shown that locally around the points (x_i, a_i) , $i = l, r$ there is a saddle-node bifurcation.

3 Homoclinic Persistence

The discussion in this section is limited to the case $b_1 < b_1^*$ and $a \in]-m(x_r), -m(x_l)[$. The objective is to apply the Melnikov's method to (2) when $f(t) = B \cos(\Omega t)$, it can be used to describe how the homoclinic orbits persist in the presence of the perturbation. For AFM models the persistence of homoclinic orbits has great practical use since it can be produce uncontrollable vibrations of the device, causing fail and generate erroneous readings, [2, 3, 23].

Before we address this problem, let us establish some notation. Consider the systems of the form

$$x' = f(x) + \epsilon g(x, t), \quad x \in \mathbb{R}^2, \quad (7)$$

where f is a vector field Hamiltonian in \mathbb{R}^2 , $g_i \in C^\infty(\mathbb{R}^2 \times \mathbb{R}/(T\mathbb{Z}))$, $i = 1, 2$, $g = (g_1, g_2)^T$ and $\epsilon \geq 0$. Now, suppose in an unperturbed system, i.e $\epsilon = 0$ in (7), the existence of a family of periodic orbits given by

$$\gamma_e = \{(x_1, x_2) : E(x_1, x_2) = e\}, \quad e \in]\alpha, \beta[,$$

such that γ_e approaches a center as $e \rightarrow \alpha$ and to an invariant curve denoted by γ_β , as $e \rightarrow \beta$. When γ_β is bounded, it is a homoclinic loop consisting of a saddle and a connection. We want to know if γ_β persists when (7), where $0 < \epsilon \ll 1$, that is, if $\gamma_\beta(t, \epsilon)$ is a homoclinic of (7) that is generated by γ_β . The first approximation of $\gamma_e(t, \epsilon)$ is given by the zeros of the Melnikov's function $M_e(t)$ defined as:

$$M_e(t) := \int_{E(x_1, x_2)=e} g_2 dx_1 - g_1 dx_2,$$

therefore, it is necessary to know the number of zeros of (3). For our purposes, the following Theorem, which is an adaptation of [11], will be useful.

Theorem 3 ([11], Theorem 6.4). *Suppose $e_0 \in]\alpha, \beta]$ and $t_0 \in \mathbb{R}$.*

1. *If $M_{e_0}(t_0) \neq 0$, then, there are no limit cycles near γ_{e_0} for $\epsilon + |t_0 + t|$ sufficiently small.*
2. *If $M_{e_0}(t) = 0$ is a simple zero there is exactly one limit cycle $\gamma_{e_0}(t_0, \epsilon)$ for $\epsilon + |t_0 + t|$ sufficiently small that approaches γ_{e_0} when $(t, \epsilon) \rightarrow (t_0, 0)$.*

Remark 1. *Melnikov's function can be interpreted as the first approximation in ϵ of the distance between the stable and unstable manifold, measured along the direction perpendicular to the unperturbed connection, that is, $d(\epsilon) := \epsilon \frac{M_\beta(t_0)}{\|f(\gamma_\beta)\|} + O(\epsilon^2)$. In particular, when $M_\beta(t_0) > 0$ (resp. < 0) the unstable manifold is above (resp. below) the stable manifold, see [10, 17] for a detail discussion.*

Rewriting (2) as a system of the form (7), we obtain

$$f(x_1, x_2) = \begin{pmatrix} x_2 \\ m(x_1) + a \end{pmatrix}, \quad g(x_1, x_2, t) = \begin{pmatrix} 0 \\ B \cos(\Omega t) - \frac{C}{x_1^3} x_2 \end{pmatrix}.$$

From Theorem 1, we have that if $b_1 < b_1^*$ and $a \in]-m(x_r), -m(x_l)[$, the unperturbed system has three equilibria from which one is a saddle, denoted by $(x_{sa}, 0)$. The function's energy associated with the conservative system is given by (4) and homoclinic loops, denoted by Γ_l and Γ_r , and $E(x_1, x_2) = E(x_{sa}, 0) = \beta$.

When calculating Melnikov's function along the separatrix on the right Γ_r , the computation along Γ_l is identical, this is:

$$\begin{aligned}
M_\beta(t_0) &= \int_{\Gamma_r} g_2 dx_1 - g_1 dx_2 = \oint_{\gamma_{\beta_r}} (E_{x_2} g_1 + E_{x_1} g_2) dt \\
&= \int_{-\infty}^{\infty} x_2(t) \left(B \cos(\Omega(t + t_0)) - \frac{C}{x_1^3(t)} x_2(t) \right) dt \\
&= B \cos(\Omega t_0) \int_{-\infty}^{\infty} \cos(\Omega t) x_2(t) dt - B \sin(\Omega t_0) \int_{-\infty}^{\infty} \sin(\Omega t) x_2(t) dt \\
&\quad - C \int_{-\infty}^{\infty} \frac{x_2^2(t)}{x_1^3(t)} dt \\
&= -2B \sin(\Omega t_0) \int_0^{\infty} \sin(\Omega t) x_2(t) dt - C \int_{-\infty}^{\infty} \frac{x_2^2(t)}{x_1^3(t)} dt.
\end{aligned}$$

Note that

$$\int_{-\infty}^{\infty} \cos(\Omega t) x_2(t) dt = 0,$$

due to $\cos(\Omega t) x_2(t)$ is an odd function. Consequently:

$$M_\beta(t_0) = -2B \sin(\Omega t_0) \int_0^{\infty} \sin(\Omega t) x_2(t) dt - C \int_{-\infty}^{\infty} \frac{x_2^2(t)}{x_1^3(t)} dt.$$

Define

$$\xi_1 = -2 \int_0^{\infty} \sin(\Omega t) x_2(t) dt, \quad \xi_2 = - \int_{-\infty}^{\infty} \frac{x_2^2(t)}{x_1^3(t)} dt,$$

and we proof that ξ_1, ξ_2 are bounded. Indeed, $dt = dx_1/x_1 = dx_1/x_2$ and $x_{sa} < x_1 < \bar{x}$ in Γ_r , where x_{sa}, \bar{x} are consecutive zeros of $E(x_1, 0) - \beta$. Now if $E(x_1, x_2) = \beta$ then

$$x_2^2 = 2 \left(\beta + ax_1 + \frac{b_2}{x_1} - \frac{b_1}{7x_1^7} - \frac{x_1^2}{2} \right),$$

hence

$$\xi_1 \leq 2 \int_0^{\infty} x_2(t) dt = 2 \int_{x_{sa}}^{\bar{x}} dx_1 = 2(\bar{x} - x_{sa}).$$

On the other hand,

$$|\xi_2| \leq 2C \int_{x_{sa}}^{\bar{x}} \left| \frac{x_2}{x_1^3} \right| dx_1 = 2C \int_{x_{sa}}^{\bar{x}} \frac{\sqrt{2 \left(\beta + ax_1 + \frac{b_2}{x_1} - \frac{b_1}{7x_1^7} - \frac{x_1^2}{2} \right)}}{|x_1^3|} dx_1 < \infty.$$

Finally Melnikov's function is rewritten as

$$M_\beta(t_0) = B \xi_1 \sin(\Omega t_0) + C \xi_2. \quad (8)$$

Theorem 4. *Under the conditions of item 2 of the Theorem 1 we have that the homoclinic orbits of (2) persist as long as ϵ is sufficiently small and:*

$$\frac{B}{C} > \left| \frac{\xi_2}{\xi_1} \right|. \quad (9)$$

Proof. Condition (9) implies that Melnikov's function (8) has a simple zero. Consequently, Theorem 3 reaches the desired conclusion. \square

Example 1. *For illustrative purposes, we have taken from [21] the realistic values of the physical parameters in Table 1. The values in Table 1 are related*

| Symbol | Value |
|--------|--------------------------------------|
| A_1 | $0.001 \times 10^{-70} \text{ Jm}^6$ |
| A_2 | $2.96 \times 10^{-19} \text{ J}$ |
| R | 10 nm |
| K | 0.87 N/m |
| Z_0 | 1.68108 nm |

Table 1: Properties of the case study of the AFM cantilever of Rützel et. al. [21]

to the following adimensionalized values b_1, b_2 and a :

$$\begin{aligned} b_1 &= 113876/10000000, & b_2 &= 148148/1000000, & a &= 1.07468, \\ |\xi_1| &= 0.290315, & |\xi_2| &= 0.382056. \end{aligned}$$

For instance, fix $C = 1$ and $\Omega = 1$, Theorem 4 guarantees that if $B > 1.316$ then the homoclinic persists.

Acknowledgments

We are grateful to anonymous referees for their useful and inspiring remarks. The authors have been financially supported by the Convocatoria Interna UTP 2016, project CIE 3-17-4.

Data Availability

The data used to support the findings of this study are included within the article.

References

- [1] A. A. Andronov, E. A. Leontovich, I.I Gordon et. al., "Qualitative Theory of Second-Order Dynamical Systems", *John Wiley and Sons*, New York, 1973.

- [2] M. Ashhab, V. Salapaka, M. Dahleh et. al., "Control of Chaos in Atomic Force Microscopes" *Proceedings of the American Control Conference*, pp. 196-202, 1997.
- [3] M. Ashhab, V. Salapaka, M. Dahleh et. al., "Melnikov-Based Dynamical Analysis of Microcantilevers in scanning Probe Microscopy" *Nonlinear Dynamics*, Vol. 20, pp. 197-229, 1999.
- [4] M. Babak and A. G. Aristides, "Compensation of Scanner Creep and Hysteresis for AFM Nanomanipulation", *IEEE Transactions on Automation Science and Engineering*, Vol. 5, No. 2, pp. 197-206, 2008.
- [5] R. Bowen and N. Hilal, "Atomic Force Microscopy in Process Engineering: Introduction to AFM for Improved Processes and Products", *Elsevier*, 2009.
- [6] B. Bhushan and O. Marti, "Nanotechnology, Scanning Probe Microscopy-Principle of operation, instrumentation, and probes", *Springer Handbook Nanotechnology*, Bhushan, Springer, Berlin, Heidelberg, pp. 573-617. 2010.
- [7] Van de B. Bram, A. Farbod and K. G. Murali, "Experimental Setup for Dynamic Analysis of Micro-and Nano-Mechanical Systems in Vacuum, Gas and Liquid", *Micromachines*, 10(3), 162, 2019.
- [8] S. G. Brush, "Interatomic forces and gas Theory from Newton to Lennard-Jones", *Archive for Rational Mechanics and Analysis*, 39(1), 1-29, 1970.
- [9] C. K. Chua and W. Y. Yeong, "3D Printing and Bioprinting in MEMS Technology", *Micromachines*, 8(7), 229, 2017.
- [10] J. Guckenheimer and P. Holmes, "Nonlinear Oscillations, Dynamical Systems, and Bifurcations of Vector Fields" *Springer*, 1986.
- [11] M. Han and P. Yu, "Normal Forms, Melnikov Functions, and Bifurcations of Limit Cycles", *Springer*, Berlin, 2012.
- [12] F. Huber and F. Giessibl, "Low noise current preamplifier for qPlus sensor deflection signal detection in atomic force microscopy at room and low temperatures". *Review of Scientific Instruments*, 88, 2017.
- [13] F. Jensen, "Introduction to Computational Chemistry", *John Wiley and Sons*, 2007.
- [14] Y. Kuznetsov, "Elements of Applied Bifurcation Theory", *Applied Mathematical Sciences*, Springer, 3rd ed. 2004.
- [15] J. E Lennard-Jones, "On the determination of molecular field. *Proc. R. Soc. Lond Ser. A Math. Phys. Eng. Sci.* 106(738), 6s"3-4477 (1924).
- [16] S. Morita, F. Giessibl, E. Meyer et. al., "Noncontact Atomic Force Microscopy", New York: *Springer*, 2015.

- [17] L. Perko L, "Differential Equations and Dynamical Systems", 3rd Edition, *Springer*, 2000.
- [18] T. O. Pleshakova, A. L Kaysheva, I. D. Shumov, et. al., "Detection of Hepatitis C Virus Core Protein in Serum Using Aptamer-Functionalized AFM Chips". *Micromachines*, 10(2), 129, 2019.
- [19] C. F. Quate and G. Binnig, "Atomic Force Microscope", *Physical Review Letters*, Vol 56, N. 9, pp. 930-934, 1986.
- [20] A. L Rachlin and G. S Henderson, "An atomic microscope (AFM) study of the calcite cleavage plane: Image averaging in Fourier space", *American Mineralogist*, Vol. 77, pp 904-910, 1992.
- [21] S. Rützel, S. I. Lee and A. Raman, "Nonlinear dynamics of atomic-force-microscope probes driven in Lennard-Jones potentials", *Proceedings of the Royal Society A*, 459, pp. 1925-1948, 2003.
- [22] M. I. Younis, "MEMS Linear and Nonlinear Statics and Dynamics", *Springer*, 2011.
- [23] W.M Zhang, G. Meng, J. B. Zhou et. al., "Nonlinear Dynamics and Chaos of Microcantilever-Based TM-AFMs with Squeeze Film Damping Effects", *Sensors* 9, pp 3854-3874, 2009.
- [24] Y. Zhang, Y. Fang, X. Zhou et. al. "Image-based hysteresis modeling and compensation for an AFM piezo-scanner", *Asian Journal of Control*, Vol 11, No. 2, pp. 166-174, 2009.